JOURNAL OF GEOPHYSICAL RESEARCH, VOL. 106, NO. A4, PAGES 5543–5549, APRIL 1, 2001

Simultaneous ground based observations of an auroral arc in daytime/twilighttime O I 630.0 nm emission and by incoherent scatter radar

D. Pallamraju, J. Baumgardner, and S. Chakrabarti

Center for Space Physics, Boston University, Boston, Massachusetts

T. R. Pedersen

Space Vehicles Directorate, Air Force Research Laboratory, Hanscom Air Force Base, Massachusetts

Abstract. We present the ground-based oxygen 630.0 nm daytime optical measurements of a discrete auroral arc from Sondre Stromfjord, Greenland. The optical measurements were made using an imaging echelle spectrograph built at Boston University. We show that the auroral optical signature extracted from the blue-sky background agrees closely in both space and time with the aurorally enhanced electron densities at 200 km altitude obtained simultaneously by the incoherent scatter radar. The dayglow measurements are also in good agreement with the integrated emission rates modeled using the measured N_e, T_e, and T_i profiles from the radar. The results reported in this paper demonstrate the potential of this spectrograph to observe aurora during daytime, and it promises to be a valuable complement to the existing tools for the investigation of upper atmospheric phenomena.

1. Introduction

Auroral emissions are the signatures of the complex magnetospheric and ionospheric interactions that take place over high-latitude upper atmosphere. The nighttime aurora has been extensively investigated over the past several decades by both ground-based and space-borne instrumentation. However, there have been very few exploratory ground-based daytime optical auroral investigations, primarily due to the presence of bright solar background continuum [*Noxon,* 1964; *Barmore,* 1977; *Cocks and Jacka,* 1979; *Pallam Raju et al.,* 1995; *Rees et al.,* 2000]. From measurements using satellite- and rocket-borne instruments, we know that the occcurrence morphology and characteristics of the daytime auroral emissions are different from those of the nighttime [*Shepherd,* 1979; *Gault et al.,* 1981; *Meng,* 1981; *Sivjee,* 1983; *Newell et al.,* 1996; *Sandholt and Farrugia,* 1999]. Some of the early measurements showed that the nighttime aurora is dominated by molecular emissions, while the daytime aurora mainly consists of atomic emissions, essentially due to differences in the energy inputs [*Meng,* 1981; *Sivjee,* 1983]. Also, a satellite-based statistical study has reported that the frequently occurring discrete aurora in the nighttime are suppressed in the daytime conditions [*Newell et al.,* 1996]. Moreover, the large-scale high-latitude plasma density structures, or the polar cap patches which are potentially capable of affecting the satellite radio communication systems, are formed in the daytime cusp region, especially when the cusp is sunlit [*Weber et al.,* 1984, 1986].

Most of our current understanding on the optical response of the cusp aurora comes from observations made when the cusp is in darkness, which occurs only near solstice at a few locations. During sunlit periods, however, as there are contrasting changes brought about in ionization, conductivities, neutral densities and temperatures, it is not known how this most dynamic region of the Earth's upper atmosphere manifests in the optical emissions. Due to lack of observations, another unknown aspect in high-latitude aeronomy is the conjugacy in auroral occurrence. Past observations have been restricted to only a few days during the equinox periods when there is simultaneous darkness over conjugate points on the globe. Being able to observe sunlit aurora in the summer hemisphere conjugate point would yield enormous information, not only on the differences in daytime versus dayside auroral occurrences, but also in a comprehensive understanding of the daytime aurora.

Optical investigations of daytime upper atmospheric phenomena using ground-based techniques have always been a challenging task due to the presence of the bright solar background continuum which is approximately 3

Paper number 2000JA000244.
0148-0227/01/2000JA000244$09.00

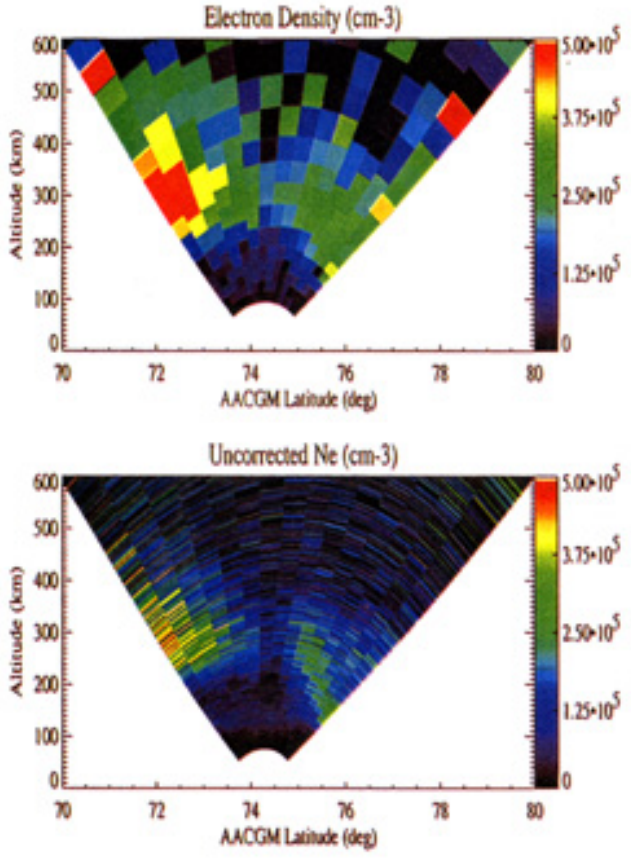

Plate 1. (top) Electron densities from a Sondre Stromfjord radar elevation scan beginning at 1758 UT. One can notice the low-altitude enhancement in electron density toward north. (bottom) Same as in the top panel, but only the returned power at higher resolution (2 km) to show the presence of an arc (uncorrected N_e in cm^{-3}). This is "uncorrected" for the effects of T_e and T_i to the spectrum, but in the present case it is expected to be nearly equal to the true electron densities. The region of auroral precipitation appears as a field-aligned density enhancement about 100 km to the north (right) of the radar site. AACGM is Altitude Adjusted Corrected Geomagnetic Coordinates.

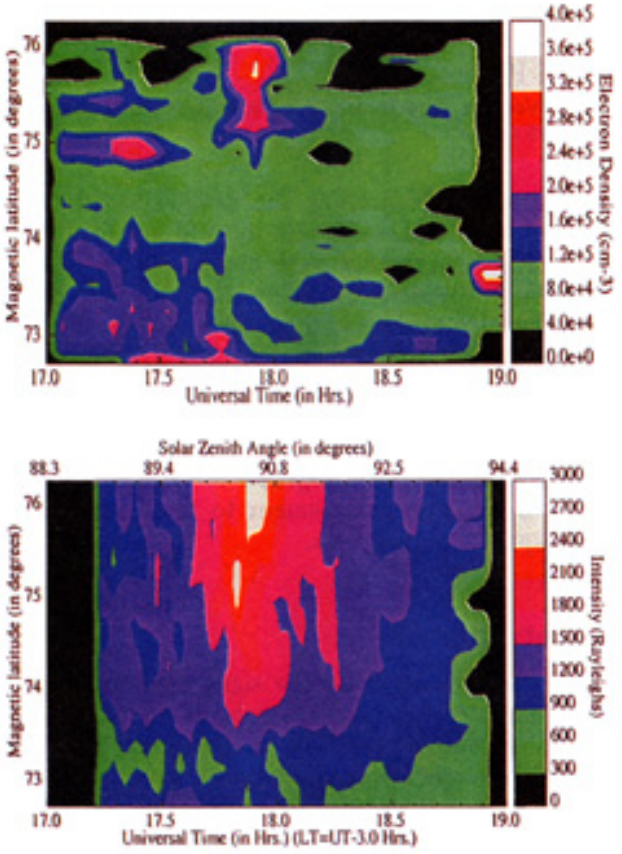

Plate 2. (a) Electron density at 200 km as obtained by the ISR at Sondre Stromfjord on January 25, 1999, shown as a contour plot with universal time and magnetic latitude. One can notice the increase in electron density beyond 74.75°N magnetic latitude, due to the occurrence of the auroral arc. (b) O I 630.03 nm airglow observations simultaneously obtained from the same location. Local time and solar zenith angle values are also shown in this panel. Notice the higher emission rates (shown in red and white) collocated with the arc occurrence as seen in 200 km electron density measurements depicted in Plate 2a. The black color in both these panels indicates the absence of data. PACE is Polar Anglo-American Conjugate Experiment. (Read 4.00e+005 as 4.00×10^5).

orders of magnitude higher in brightness [*Cocks et al.*, 1980]. Using a spectral scanning polarimeter, *Noxon* [1964] reported the first O I 630.0 nm dayglow observations from Boston, although the emission values were unusually high (50 KR) for the magnetically quiet conditions. *Bens et al.* [1965], *Barmore* [1977], *Cocks and Jacka* [1979], *Greet et al.* [1989], and *Rees et al.* [2000] have used multi etalon Fabry-Perot interferometers to obtain dayglow emissions. *Narayanan et al.* [1989] and *Sridharan et al.* [1998] described a method of obtaining dayglow emissions by using a single Fabry-Perot etalon in conjunction with a novel mask system [*Sridharan et al.*, 1993]. Using this instrument, *Pallam Raju et al.* [1995] presented relative auroral emission rate variations at various wavelengths from Antarctica which showed an increase in the N_2^+ and H_β emissions in response to a geomagnetic storm event.

None of the earlier measurements had the benefit of simultaneous incoherent scatter radar (ISR) measurements which yield useful information on the altitude structure of the background ionospheric conditions. In this paper we report on ground-based O I 630.0 nm observations carried out as a part of the multi-instrument high-latitude plasma structures (HLPS) campaign carried out over several weeks in January 1999. One of the aims of the HLPS campaign was to use the High-Resolution Imaging Spectrograph using Echelle grating (HIRISE) to investigate the presence and formation of these structures by observing the daytime airglow emissions and to observe optical emissions in the daytime cusp. Unfortunately, unusually bad weather throughout the campaign period hampered the dayglow observations, except for only 2 hours in the post noon sector on January 25, 1999. A significant auroral event was observed during this period. In this paper we present the first O I 630.0 nm dayglow/twilightglow measurements of an auroral arc simultaneously verified by the ISR data from Sondre Stromfjord radar. The observed auroral arc never approached close enough to the site for an E region electron density profile to be obtained, which would have allowed an estimation of the precipitating particle energy and flux. Integrated O I 630.0 nm emission rates estimated using the ISR measured N_e, T_e, and T_i altitude profiles show reasonably good agreement with the observed dayglow. These results demonstrate the potential of HIRISE in carrying out continuous round-the-clock auroral measurements.

2. Measurement Technique and Data Analysis

HIRISE is a long-slit Echelle spectrograph (slit length of 40 mm) that can simultaneously observe many spectral features located anywhere in the visible spectrum. It uses an interference filter (placed behind the slit) which allows only 10 nm spectral bandwidth of light centered around 630.0 nm and a 1 K x 1 K back-thinned CCD detector to record the high-resolution spectrum. It has $f/11$ input optics and attains a dispersion and resolution of 0.004 nm/pixel and 0.012 nm, respectively, at 589.3 nm, and it is capable of retrieving dayglow emission features buried in the bright solar background continuum [*Chakrabarti*, 1998; *Pallamraju et al.*, 2000]. During the present campaign, a fish eye lens (of focal length 15 mm) was placed in front of the slit to yield a field of view of about 180° along the slit and 0.5° perpendicular to it. The slit was aligned along the magnetic north-south direction, and hence the image thus obtained contained spatial information along this orientation. With a knowledge of (or assumption about) the emission altitude, different sections along the imaging direction have been mapped to their corresponding latitudes.

The procedure to obtain the dayglow and daytime auroral emissions using HIRISE is to compare the high-resolution sky and solar spectra. As the solar spectrum does not consist of any contribution due to the Earth's atmospheric emissions, the difference between the sky and solar spectra would yield contributions due to thermospheric dayglow emission (and daytime auroral contribution, if any) and the Ring effect [*Grainger and Ring*, 1962]. (Ring effect refers to the "filling in" of the solar Fraunhofer absorption lines produced mainly by sunlight scattering off the molecules of the Earth's atmosphere). We are able to subtract these two scaled spectra because they have been obtained by the same instrument with identical instrumental parameters for both data sets [*Pallamraju et al.*, 2000].

In order to estimate the absolute values of the dayglow emission rates, we scaled the solar and blue-sky images with an image obtained by using a standard (calibrated) lamp. The solar spectrum along the imaging direction is divided into different sections. Each section consists of slant column integrated emissions along their view angles. The "reference solar spectra" obtained by averaging all the rows (spatial elements on the CCD image) at each section are scaled with those of the corresponding sections from the sky spectra by a least squares technique to match the continuum regions on either side of the emission wavelength. The difference between such scaled solar spectrum and the blue-sky spectrum would yield information on the atmospheric contribution (dayglow emission and Ring effect contribution).

ISR measurements were made in a mode comprised of alternating azimuth and elevation scans. Here we have used only the elevation scan data, which was aligned along the magnetic north-south direction, for comparison with dayglow observations. Each elevation scan extended down to 45° above the horizon, covering about 3° latitude range at an altitude of 200 km, and was completed in approximately 2 min. The elevation scan data were divided into eight different angle bins to approximate as closely as possible to those of the optical measurements. As the azimuth scan also took around 2 min to complete, the temporal spacing between two

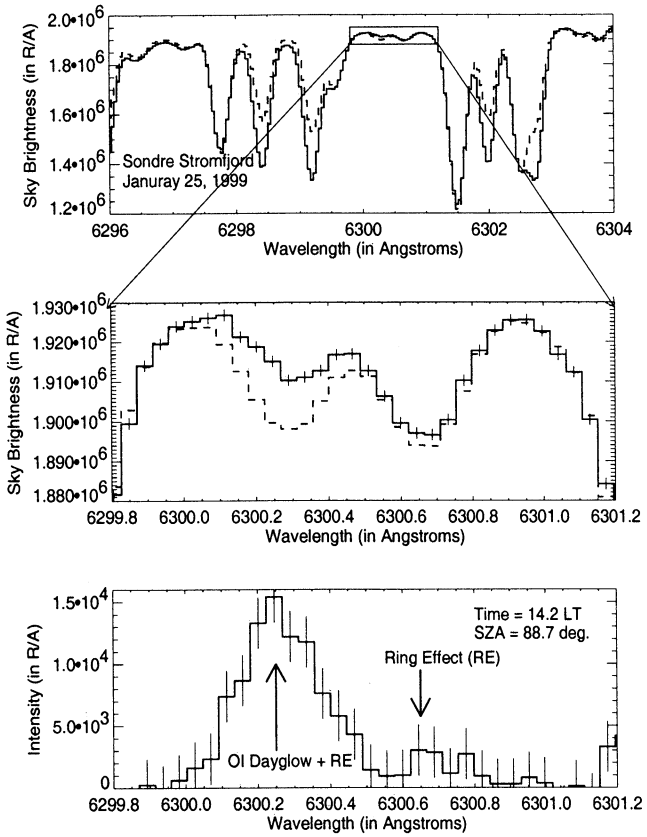

Figure 1. (top) Typical blue-sky (solid line) and scaled solar (dashed line) spectra obtained from Sondre Stromfjord along with $\pm 1\sigma$ variation. (middle) The region of interest around 630.0 nm is blown up. (bottom) The difference between the blue-sky and solar spectra depicting the O I 630.03 nm dayglow as well as the Ring effect contributions.

successive ISR data points at a given elevation angle is around 4 min.

3. Observations

Observations were carried out from Sondre Stromfjord Incoherent Scatter Radar Facility in Kangerlussuaq, Greenland (67.0°N, 51.0°W) during January 1999. During this period the Sun was above the horizon during 1300-1800 UT. The magnetic latitude (74.5°N) of the Sondre Stromfjord makes it a site with high probability of being directly under the geomagnetic cusp near magnetic noon. The only cloud-free daytime optical measurements during the campaign were available between 1700 and 1900 UT (1400 and 1600 LT) on January 25, 1999. Exposure times for obtaining the blue-sky images varied from 1.5 to 8 min.

Figure 1 shows the typical spectra obtained from Sondre Stromfjord. The top panel shows the blue-sky (solid line) and the scaled solar spectra (dashed line). The spectral region of interest is blown up and is depicted in the middle panel. Notice that the blue-sky spectrum is "filled in" at 630.03 and 630.07 nm regions as compared to the solar spectrum. The blue-sky spectral region at 630.03 nm consists of both the dayglow emission and the Ring effect contribution. O I 630.0 nm dayglow emission mechanisms have been reviewed by *Hays et al.* [1978]. For auroral latitudes they are (1) photoelectron impact on atomic oxygen, (2) photodissociation of O_2, (3) dissociative recombination of O_2^+, (4) excitation by thermal electrons, and (5) excitation by particle precipitation. The Ring effect, on the other hand, is believed to be mainly due to rotational Raman scattering of solar photons by atmospheric molecules [*Brinkmann,* 1968], which affects all the Fraunhofer absorption regions. From Figure 1 it can be seen that the 630.0 nm oxygen emission occurs in a Fraunhofer absorption region. Hence to obtain the dayglow emission contribution, it is important to remove the contribution of the Ring effect from the 630.03 nm Fraunhofer absorption region in the blue-sky spectrum. In our approach the Ring effect contribution at 630.03 nm region is assumed to be equal to that at the 630.07 nm, as this region (1) is not known to contain any atmospheric emission contribution, (2) is spectrally close to the 630.03 nm region, and (3) is of nearly the same absorption line strength as at 630.03 nm region [*Pallamraju et al.,* 2000]. The difference in the blue-sky and the solar spectra is shown in the bottom panel of this figure. The area under the curve at 630.07 nm is estimated and is subtracted from the one at 630.03 nm to obtain only the oxygen 630.03 nm dayglow emission contribution. This process is repeated for each section of the image at different times to obtain integrated dayglow emissions as a function of latitude and universal time.

The top panel of Plate 1 shows electron densities in the plane of the elevation scan of ISR which began at 1758 UT. These values are averaged in a height range of 48 km. One can notice a low-altitude ionization towards north indicating an aurora. To bring out the contrast better, we show in the bottom panel of this figure the "power profile" or "uncorrected" (only the returned power not correcting for the effect of T_e and T_i to the spectrum) estimate of electron densities obtained at 2 km resolution. For this period, as the T_i was high and approached T_e, it is expected that this returned power is proportional to the electron densities. An auroral arc can clearly be seen as a field-aligned enhancement (but moving toward north) in the uncorrected electron density at a distance of about 100 km north (to the right in the figure) of the radar site. This scan represents the closest approach of the arc to the radar site, but because of the 45° minimum elevation constraint of the scan, no radar data are available below about 150 km altitude at the location of the arc.

Electron densities from ISR elevation scans for 200 km altitude are shown as a function of UT and magnetic latitude in Plate 2a for the period when optical data are available. As can be seen in this figure, enhancement in plasma densities due to auroral arc oc-

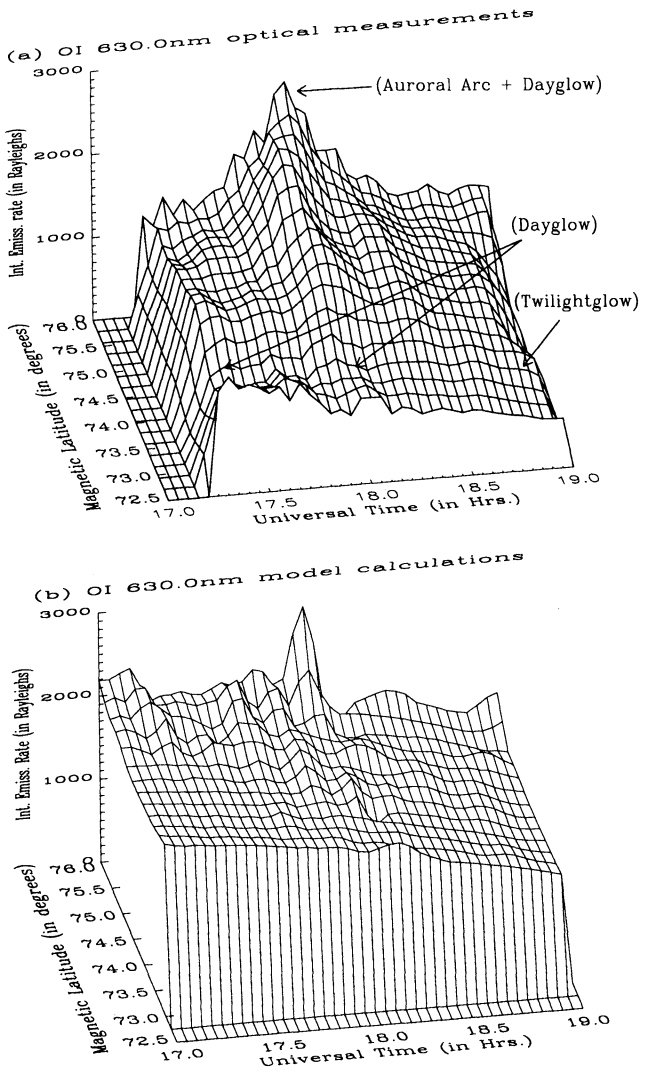

Figure 2. (a) O I 630.0 nm dayglow/twilightglow measurements from Sondre Stromfjord using HIRISE. As compared to the "ambient" emission level, notice relatively higher emission rates in the region between 74.5°N and 76.0°N magnetic latitude and in the time zone between 17.7 and 18.1 UT, which is the same in spatial and temporal extent of the auroral arc occurrence as seen in the electron densities (Plate 2a). (b) Column-integrated O I 630.0 nm model emission rates obtained using the /glow model for the same time and latitude extent as for the measurements shown in Figure 2a. Measured profiles of N_e, T_e, and T_i by ISR and model (MSIS) neutral densities have been used for these calculations. Notice the overall similarity in variations between the two panels.

curred for a few minutes between 17.7 and 18.1 UT in the northern half of the field of view (magnetic latitude region of 74.6° – 76.0°N). The electron density enhancement reached a maximum near 76.0°N before 1800 UT. Plate 2b shows the contour plot of the measured O I 630.03 nm dayglow/twilightglow column-integrated emission rates obtained simultaneously from the same location using HIRISE. Local time and the corresponding solar zenith angle (SZA) values are also shown. Plate 2b shows an emission enhancement (shown in red and white) in the optical measurements at the same time and location as electron density enhancement in Plate 2a indicating the optical response to the auroral arc.

Figure 2a shows an alternative representation of the dayglow measurements between 1700 and 1900 UT. There is a monotonic decrease in the emission rate with time, as can be expected due to decrease in the solar flux induced sources of O I 630.0 nm emission with increase in SZA. The maximum uncertainties in the integrated emission rates are around 140 R (20%) at 1715 UT, which monotonically decrease to around 20 R (0.2%) by 1900 UT. Van Rhijn advantage for slant columns has not been taken into account as the emission layer is not uniform. Hence a comparison is made with model estimates carried out along a similar view geometry. Emission rate in the northern regions are 30-40% higher than those in the southern magnetic latitudes. It is striking to note that the region between 74.5° and 76.0°N magnetic latitude records relatively higher emissions as compared to the "ambient" emission level during the time period between 17.7 and 18.1 UT, exactly in the same location where the auroral arc was seen in the ISR observations (see Plate 2a). This ambient emission level is the dayglow emission contribution (without the contribution due to the auroral arc). Hence it is possible to obtain the O I 630.0 nm contribution due to the auroral arc by subtracting the smoothly varying dayglow emissions. Figure 2b shows the integrated O I 630.0 nm airglow emission rates along the view direction calculated using the /glow model [*Solomon and Abreu*, 1989]. Measured N_e, T_e, and T_i profiles derived by the ISR have been carefully filtered to avoid bad data and then used as inputs for the /glow model while the neutral density and temperature values are model (Mass Spectrometer Incoherent Scatter, MSIS) generated. The model 630.0 nm emission rates, too, show a monotonic decrease with time (increasing SZA), similar to the optical measurements. These values show an increase in a region north of 75.0°N magnetic latitude with a peak at about 76.0°N around 1800 UT. The strong variations in the emission rates in the region is similar in spatial and temporal extent to the occurrence of the auroral arc, which is registered as the enhancement in emission rates of the dayglow observations (Plate 2b and Figure 2a).

4. Discussion

The dayglow measurements and the model calculations shown in Figures 2a and 2b depict many similarities, especially in the time and location of the occurrence of the auroral arc as seen in electron densities (Plate 2a). Given such independent approaches that resulted in Figures 2a and 2b, the agreement between them is very encouraging. However, there are some dif-

ferences between them. The observations show temporal structures throughout the latitude region and also show 30-40% more emissions toward 76.0°N magnetic latitude as compared to the ones at 73.0°N. In comparison, the model calculations do not show such steep gradient in emission rate from north to south and show only a sharp peak at about 76.0°N magnetic latitude around 1800 UT. These discrepancies could be due to a combination of the possibilities discussed below.

As mentioned earlier, the estimates of particle flux and energies associated with the occurrence of the arc were not available, and hence this contribution could not be included in the O I 630.0 nm model calculations, which, we believe, could be mainly responsible for the discrepancies. There are other possibilities as well which could partly contribute to the discrepancies between the observed and model emissions. The optical measurements recorded in directions other than zenith are due to the integrated dayglow emissions along a slant column. We estimated the N_e, T_e, and T_i profiles along similar slant columns corresponding to the observations. But given the nature of the radar movement in fixed time intervals (or fixed angular ranges), it is possible, especially in a region where particle precipitation is occurring, that small changes in angles of integration could bring about a change in the overall magnitudes of the modeled emissions. In addition, while the dayglow measurements are continuous in both space and time, the model calculations performed are discrete in both space and time due to the movement of the ISR. Hence the former represents an integrated effect in both space and time. Moreover, it should be kept in mind that while the dayglow observations are a result of variations in both the neutral and plasma parameters, the calculations are performed using measured plasma parameters and model (MSIS) neutral parameters. It is known that MSIS [*Hedin,* 1987] represents average values of neutral parameters for a given local time and location but does not show small-scale variabilities, especially due to the arc occurrence as seen in the present study. Therefore it is not unimaginable that the model emission rates do not show an increase toward northern latitudes corresponding to the energy inputs (due to the arc occurrence) as opposed to the measurements.

In spite of the possible differences between the measurements and the model calculations as described above, the agreement between them and with the electron densities at 200 km is remarkably good. To emphasize this and also to examine the temporal variations between the measurements and model estimates, we compare only near-zenith (zenith angles of 88.4° – 94.0°) emission rates in Figure 3 which eliminates the effects of horizontal structure along the line of sight. It can be seen that both the optical measurements and the calculations show a monotonic decrease in emission rates from 1700 to 1900 UT. One can also notice that the temporal structure seen in the optical measurements at 17.9 UT has a correspondence in the calculations, albeit not as prominent. Further, the observations show

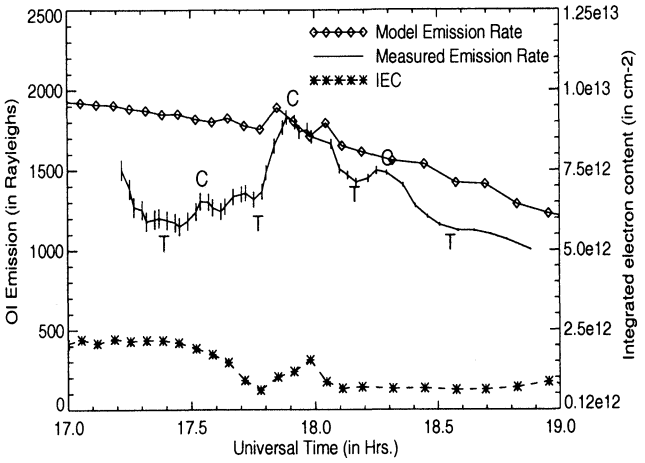

Figure 3. Measured and model O I 630.0 nm dayglow emission rates from Sondre Stromfjord. The $\pm 1\sigma$ error bars are also depicted for the measurements. Integrated electron content (IEC) between 180 and 400 km is also shown. One can notice the "crests" (C) and "troughs" (T) in the measured dayglow emissions which are possible manifestations of the atmospheric gravity waves. Such a wave structure is not seen in the integrated electron content. (Read 1.25e13 as 1.25×10^{13}).

a wave-like periodicity of around 24 min with "troughs" and "crests" in the emission rates (marked as T and C in Figure 3). As the spatial distribution in neutral density brought about by gravity waves can, in turn, modulate the airglow volume emission rates [*Krassovsky,* 1972], it is possible that the periodic behavior seen in dayglow observations could be of gravity wave origin induced due to the auroral occurrence around 76.0°N magnetic latitude. It is interesting to note that there is an asymmetry in the wave shape. The average time taken between the apparent trough to crest formation is 8.4 min, while between the crest to trough it takes 15 min. Column-integrated electron densities (between 180 and 400 km) for the same times and along similar columns as for optical observations are also shown in Figure 3. As the integrated electron content does not show such fluctuations, we interpret this periodic behavior to be of the class of atmospheric gravity waves (waves that are not strong enough to produce corresponding modulations in ionospheric parameters). Atmospheric gravity waves of such scale sizes (660 km) are not uncommon in these latitude regions and have been observed by other measurements during such auroral events [*Hocke and Schlegel,* 1996, and references therein]. It is therefore not surprising that the model estimates do not show the shallow valley that is observed in the measurements between 17.3 and 17.6 UT as (also mentioned above) the neutral density values used for calculations are model generated. More such concerted and coordinated campaigns in the future would help in understanding the thermospheric behavior during particle precipitation events at the cusp locations during sunlit conditions.

5. Conclusion

A new instrument called the High-Resolution Imaging Spectrograph using Echelle grating has been built for the investigation of daytime upper atmospheric phenomena. During observations from Sondre Stromfjord in Greenland, this instrument detected a significant enhancement in O I 630.0 nm dayglow emissions which correspond closely in space and time to the auroral arc observed simultaneously by the incoherent scatter radar. The observed dayglow agrees reasonably well with the model calculations carried out by the /glow model using the measured N_e, T_e, and T_i values as inputs. The optical measurements also registered wavelike modulations in emissions which are possibly due to atmospheric gravity waves generated in association with the occurrence of the auroral arc. The success of this technique opens up many new possibilities for continuous airglow studies similar to radar observations.

Acknowledgments. The January 1999 HLPS campaign was dedicated to the memory of the late Edward Weber. Support to deploy HIRISE at Sondre Stromfjord was provided by AFRL. We thank Stanley Solomon for providing us with the /glow model. We thank Jeffrey Thayer for providing the radar data. This work was supported by NSF grant ATM 9601846. Work at the Air Force Research Laboratory was supported by AFOSR task 2310G904. Finally, we highly appreciate the local support of the site crew at Sondre Stromfjord.

Janet G. Luhmann thanks Gordon Shepherd and another referee for their assistance in evaluating this paper.

References

Barmore, F. E., High resolution observations of the 6300 Å oxygen line in the day airglow, *Planet Space Sci., 25*, 185-191, 1977.

Bens, A. R., L. L. Cogger, and G. G. Shepherd, Upper atmospheric temperatures from Doppler line widths, III, Observations of the OI dayglow emission at 6300 Å, *Planet Space Sci., 13*, 551-563, 1965.

Brinkmann, R. T., Rotational Raman scattering in planetary atmospheres, *Astrophys. J., 154*, 1087-1093, 1968.

Chakrabarti, S., Ground-based spectroscopic studies of sunlit airglow and aurora, *J. Atmos. Sol. Terr. Phys., 60*, 1403-1423, 1998.

Cocks, T. D., and F. Jacka, Daytime thermospheric temperatures, wind velocities and emission intensities derived from ground-based observations of the OI 630.0 nm airglow line profile, *J. Atmos. Terr. Phys., 41*, 409-415, 1979.

Cocks, T. D., D. F. Creighton, and F. Jacka, Application of a dual Fabry-Perot spectrometer for daytime airglow studies, *J. Atmos. Terr. Phys., 42*, 499-511, 1980.

Gault, W. A., R. A. Koehler, R. Link, and G. G. Shepherd, Observations of the optical spectrum of the dayside magnetospheric cleft aurora, *Planet Space Sci., 29*, 321-333, 1981.

Grainger, J. F., and J. Ring, Anomalous Fraunhofer line profiles, *Nature, 193*, 762, 1962.

Greet, P., M. Conde and F. Jacka, Daytime observation of sodium layer with a Fabry-Perot spectrometer at Mawson, *Geophys. Res. Lett., 16*, 871-874, 1989.

Hays, P. B., D. W. Rusch, R. G. Roble, and J. C. G. Walker, The OI (6300 Å) airglow, *Rev. Geophys., 16*, 225-232, 1978.

Hedin, A. E., MSIS-86 thermospheric model, *J. Geophys. Res., 92*, 4649-4662, 1987.

Hocke, K., and K. Schlegel, A review of atmospheric gravity waves and traveling ionospheric disturbances: 1982-1995, *Ann. Geophys., 14*, 917-940, 1996.

Krassovsky, V. I., Infrasonic variations of OH emission in the upper atmosphere, *Ann. Geophys., 28*, 739-746, 1972.

Meng, C.-I., Electron precipitation in the midday auroral oval, *J. Geophys. Res., 86*, 2149-2174, 1981.

Narayanan, R., J. N. Desai, N. K. Modi, R. Raghavarao, and R. Sridharan, Dayglow photometry: A new approach, *Appl. Opt., 28*, 2138-2142, 1989.

Newell, P. T., C.-I. Meng, and K. M. Lyons, Suppression of discrete aurorae by sunlight, *Nature, 381*, 766-767, 1996.

Noxon, J. F., A study of the 6300Å oxygen line in the day airglow, *J. Geophys. Res., 69*, 3245-3255, 1964.

Pallam Raju, D., R. Sridharan, R. Narayanan, N. K. Modi, R. Raghavarao, and B. H. Subbaraya, Ground-based optical observations of daytime auroral emissions from Antarctica, *J. Atmos. Terr. Phys., 57*, 1591-1597, 1995.

Pallamraju, D., J. Baumgardner, and S. Chakrabarti, A multiwavelength investigation of the Ring effect in the day sky spectrum, *Geophys. Res. Lett., 27*, 1875-1878, 2000.

Rees, D., M. Conde, A. Steen, and U. Brandstrom, The first daytime ground-based optical image of the aurora, *Geophys. Res. Lett., 27*, 313-316, 2000.

Sandholt, P. E., and C. J. Farrugia, On the dynamic cusp aurora and IMF B_y, *J. Geophys. Res., 104*, 12,461-12,472, 1999.

Shepherd, G. G., Dayside cleft aurora and its ionospheric effects, *Rev. Geophys., 17*, 2017-2033, 1979.

Sivjee, G. G., Differences in near UV ($\sim 3400 - 4300$ Å) optical emissions from midday cusp and nighttime auroras, *J. Geophys. Res., 88*, 435-441, 1983.

Solomon, S. C., and V. Abreu, The 630 nm dayglow, *J. Geophys. Res., 94*, 6817-6824, 1989.

Sridharan, R., R. Narayanan, N. K. Modi, and D. Pallamraju, A novel mask design for multiwavelength dayglow photometry, *Appl. Opt., 32*, 4178-4180, 1993.

Sridharan, R., N. K. Modi, D. Pallamraju, R. Narayanan, T. K. Pant, A. Taori, and D. Chakrabarty, A multiwavelength daytime photometer: A new tool for the investigation of atmospheric processes, *Meas. Sci. Technol., 9*, 585-591, 1998.

Weber, E. J., J. Buchau, J. G. Moore, J. R. Sharber, R. C. Livingston, J. D. Winningham, and B. W. Reinisch, *F* layer ionization patches in the polar cap, *J. Geophys. Res., 89*, 1683-1694, 1984.

Weber, E. J., J. A. Klobuchar, H. C. Carlson, Jr., R. C. Livningston, O. de la Beaujardiere, M. McCready, J. G. Moore, and J. D. Bishop, Polar cap *F* layer patches: Structure and dynamics, *J. Geophys. Res., 91*, 12,121-12,129, 1986.

J. Baumgardner, S. Chakrabarti, and D. Pallamraju, Center for Space Physics, 725 Commonwealth Avenue, Boston University, Boston, MA 02215. (jeff@spica.bu.edu; supc@bu.edu; dpraju@bu.edu)

T. R. Pedersen, Space Vehicles Directorate, Air Force Research Laboratory, 29 Randolph Road, Hanscom, AFB, MA 01731. (Todd.Pedersen@hanscom.af.mil)

(Received June 23, 2000; revised September 29, 2000; accepted October 2, 2000.)